

UNCLASSIFIED

AD NUMBER

AD478873

LIMITATION CHANGES

TO:

Approved for public release; distribution is unlimited.

FROM:

Distribution authorized to U.S. Gov't. agencies and their contractors; Critical Technology; MAR 1966. Other requests shall be referred to Arnold Engineering Development Center, Attn: AETI, Arnold AFS, TN 37389. This document contains export-controlled technical data.

AUTHORITY

AEDC ltr, 23 Jan 1975

THIS PAGE IS UNCLASSIFIED

MAR 30 1966
APR 19 1966

0.2



HEAT-TRANSFER MEASUREMENTS ON A SATELLITE CONFIGURATION AND SHROUDED DISK

J. T. Miller
ARO, Inc.

PROPERTY OF U. S. AIR FORCE
AEDC LIBRARY
AF 40(600)1200

March 1966

This document has been approved for public release

its distribution is unlimited. *A7 letter 1/23/75*
signed W.D. Cole

This document is subject to special export controls
and each transmittal to foreign governments or foreign
nationals may be made only with prior approval of
Arnold Engineering Development Center (AETC).

**VON KÁRMÁN GAS DYNAMICS FACILITY
ARNOLD ENGINEERING DEVELOPMENT CENTER
AIR FORCE SYSTEMS COMMAND
ARNOLD AIR FORCE STATION, TENNESSEE**

NOTICES

When U. S. Government drawings specifications, or other data are used for any purpose other than a definitely related Government procurement operation, the Government thereby incurs no responsibility nor any obligation whatsoever, and the fact that the Government may have formulated, furnished, or in any way supplied the said drawings, specifications, or other data, is not to be regarded by implication or otherwise, or in any manner licensing the holder or any other person or corporation, or conveying any rights or permission to manufacture, use, or sell any patented invention that may in any way be related thereto.

Qualified users may obtain copies of this report from the Defense Documentation Center.

References to named commercial products in this report are not to be considered in any sense as an endorsement of the product by the United States Air Force or the Government.

HEAT-TRANSFER MEASUREMENTS ON A SATELLITE
CONFIGURATION AND SHROUDED DISK

J. T. Miller
ARO, Inc.

This document is subject to special export controls and each transmittal to foreign governments or foreign nationals may be made only with prior approval of Arnold Engineering Development Center (AETI).

FOREWORD

The work reported herein was sponsored by Arnold Engineering Development Center (AEDC), Air Force Systems Command (AFSC), for the General Electric Company, under Program Element 65402234.

The results of tests presented were obtained by ARO, Inc. (a subsidiary of Sverdrup and Parcel, Inc.), contract operator of the AEDC, AFSC, Arnold Air Force Station, Tennessee under Contract AF40(600)-1200. The test was conducted from December 6 to 31, 1965, under ARO Project No. VL0642, and the manuscript was submitted for publication on January 31, 1966.

This technical report has been reviewed and is approved.

John W. Hitchcock
Major, USAF
AF Representative, VKF
DCS/Test

Jean A. Jack
Colonel, USAF
DCS/Test

ABSTRACT

This report presents heat-transfer measurements made on a typical satellite configuration in testing environments which simulate conditions at approximately 60 miles altitude, depending on full-scale vehicle size and the particular simulation parameter chosen. The total heating loads to various individual segments of the complete model are tabulated, and a heat-transfer distribution is proposed on the basis of the experimental results. Also reported are measurements on the effect of the extent of a cooled shroud on the heat transfer to a disk normal to the flow.

CONTENTS

	<u>Page</u>
ABSTRACT	iii
NOMENCLATURE	vi
I. INTRODUCTION	1
II. APPARATUS	
2.1 Wind Tunnel	1
2.2 Test Conditions	2
2.3 Altitude Simulation	2
2.4 Models	2
III. EXPERIMENTAL PROCEDURES AND RESULTS	3
IV. CONCLUSIONS	5
REFERENCES	6
APPENDIXES	
I. Tunnel L	27
II. Effect of Density Ratio on Second-Order Stagnation Region Heating Rate and Skin Friction	35

ILLUSTRATIONS

Figure

1. Satellite Model	7
2. Shrouded Disk.	7
3. Photograph of Test Models	8
4. Altitude versus Satellite Diameter for Knudsen Number Simulation	9
5. Altitude versus Viscous Interaction Parameter for Various Satellite Diameters	10
6. Sketch of Model with Spherical Cap Forebody.	11
7. Forebodies Used to Obtain Segments of Total Heating Distribution	11
8. Sketch of Shrouded Disk Probe	12
9. Progressive Removal of Shroud.	12
10. Thermal Conductivity of Copper.	13
11. Measured Heat Flux Referenced to Cold Wall.	14

<u>Figure</u>		<u>Page</u>
12.	Measured Heat Flux to Shrouded Disk Referenced to Cold Wall	15
13.	Total Heating Rate to a Spherical Segment	16
14.	Comparison of Present Data with Previous Data and Theories	17
15.	Distribution of Heating Rate to Satellite Model: Condition I	18
16.	Distribution of Heating Rate to Satellite Model: Condition II	19
17.	Total Heating Rate to a Spherically Blunted Cone	20
18.	Heat-Transfer Rate to a Flat Nose	21

TABLES

I.	Test Conditions	23
II.	Measured Values of Heating Rate to Segments of Satellite Vehicle, Referenced to Cold Wall	24
III.	Measured Values of Heating Rate to Shrouded Disk, Referenced to Cold Wall	25

NOMENCLATURE

A	Area
a	Extent of shroud (see Fig. 9)
C_{∞}	$\mu_w T_{\infty} / \mu_{\infty} T_w$
D	Diameter
d	Diameter of probe stem (see Fig. 6)
FM	Free molecular theory
H_0	Total enthalpy
H_w	Model wall enthalpy
K	Thermal conductivity
Kn_{∞}	Knudsen number in free stream

L	Total length of model
ℓ	Distance between thermocouples (see Fig. 6)
M_∞	Free-stream Mach number
p_o	Total pressure
p_o'	Impact pressure
p_∞	Free-stream static pressure
\dot{Q}	Total heating rate
q_∞	Free-stream dynamic pressure
\dot{q}	Local heat-transfer rate
\dot{q}_o	Stagnation point heat-transfer rate
\dot{q}_{of-r}	Stagnation point heat transfer as computed by method of Fay and Riddell (Ref. 5)
Re_∞, R_n	Free-stream Reynolds number (based on nose radius)
Re_∞, L	Free-stream Reynolds number (based on axial length of body)
Re_2	Reynolds number behind assumed Rankine-Hugoniot type of normal shock (based on R_n or $D/2$, as shown)
R_n	Nose radius of curvature
S	Distance along body (from stagnation point)
T_1	Temperature measured at forward thermocouple
T_2	Temperature measured at rear thermocouple
T_{aw}	Adiabatic recovery temperature on model wall
T_o	Total temperature
T_w	Model wall temperature
T_∞	Free-stream static temperature
U_∞	Free-stream velocity
x	Distance from nose measured along axis
θ	Angle between axis and the normal to the surface on a spherical shape
θ_c	Cone angle
λ_∞	Free-stream mean free path

μ_w	Viscosity evaluated at T_w
μ_∞	Viscosity evaluated at T_∞
ρ_2	Density behind normal shock
ρ_∞	Free-stream density

SECTION I INTRODUCTION

The prediction of the forces and heating loads encountered during the flight of a satellite in a highly eccentric orbit is a problem difficult to solve by analytic means. The flow conditions may span the whole regime, from free molecular to continuum flow. From a computational standpoint, the most uncertain is the transitional flow regime between these two extremes. There are two motives for obtaining experimental data in this flow regime; first, the heating load to a typical vehicle configuration can be inferred from direct experimental measurements performed on a model under suitably controlled conditions, and, secondly, experimental data provide a guide for the development of theoretical methods of predictions.

The experimental heat-transfer data reported here were measured on a model of a typical low-earth-orbit satellite vehicle at simulated altitudes of 308,000 and 330,000 ft (based on an assumed 6-ft-diam full-scale body and matching of Kn_∞ values). Specifically, the shape consisted of a 10-deg spherically blunted cone followed by a 20-deg cone frustum, and a cylindrical afterbody. This model is shown in Fig. 1.

As an additional part of the test, the heat transfer to a shrouded disk was also investigated. This configuration is shown in Fig. 2. The shroud was progressively removed so that the effect of the amount of shroud extension could be obtained. Figure 3 is a photograph of the models. Force measurements have been previously reported for the satellite model in Ref. 1.

SECTION II APPARATUS

2.1 WIND TUNNEL

The low density hypervelocity tunnel (Gas Dynamic Wind Tunnel, Hypersonic (L)) used to obtain these data is a continuous-type, arc-heated tunnel, using nitrogen for this particular test. A complete description is given in Appendix I together with the operational capabilities.

2.2 TEST CONDITIONS

The flow conditions used in these tests are tabulated in Table I. The two axisymmetric nozzles used to produce these flows are contoured and have gradient-free test sections. This uniform-flow portion of the nozzle is approximately 2 in. in diameter and 6 in. long for the higher Reynolds number nozzle. The two particular test conditions were chosen primarily because of the variation of Knudsen number represented (approximately a factor of three).

2.3 ALTITUDE SIMULATION

Figure 4 gives the altitude (using atmospheric data from Ref. 2) simulated by the satellite model at the present test conditions when Kn_∞ is matched. Figure 5 shows the altitude as a function of vehicle diameter and the viscous interaction parameter, $M_\infty \sqrt{C_\infty / Re_{\infty, L}}$, along with the value of this parameter for the two test conditions. Additionally, it may be calculated that the altitude simulation, based on matching Re_∞ , R_n for an assumed 6-ft-diam full-scale satellite, corresponded to heights of 340,000 and 318,000 ft above Earth for flow conditions I and II, respectively. The cold-wall condition ($T_w \ll T_o$), so important in tests of this type, also was effectively simulated.

2.4 MODELS

Several models were used to obtain the data reported herein. The individual models were designed so that the heat flux which entered a specified portion of the model was constrained to flow through a constant-diameter cylindrical stem in order to reach the cooling water jacket (see Fig. 6). The heat flux was then obtained by measuring the steady-state temperature gradient along this stem with two thermocouples. Four separate satellite models were used, all with the same overall configuration, but each with a different extent of the forebody instrumented to give the cumulative heating load from the nose back to a particular location. Sketches showing the instrumented sections of these models are shown in Figs. 6 and 7.

For the shrouded disk model, the same basic instrumentation scheme was followed, but only one model was used, with the shroud being progressively removed so that the data obtained constituted a parametric study of the effect of shrouding. The internal arrangement and various configurations of this model are shown in Figs. 8 and 9. It should be noted that the shroud was cooled (cf Fig. 8).

SECTION III EXPERIMENTAL PROCEDURES AND RESULTS

The various models (see Figs. 7 and 9) were each installed in the test section, and the temperature data were recorded after a steady-state condition had been attained. The time required for steady-state temperatures to be realized was from 10 to 30 sec. These temperatures were recorded, approximately one set per minute for from 10 to 20 min, to ensure that the data were consistent and to determine if a dependency on time of exposure existed. It was observed that the probe accumulated foreign matter during testing, which consistently increased the measured heating rate to a maximum after about 40 min. Cleaning the probe removed the accumulation and restored the data to their initial values. Inasmuch as the rate of change was much less than the time needed to acquire the initial, "nearly clean" data, the probe was cleaned often, and the data reported are for a nominally clean copper surface.

The heat flow was restrained to be essentially one-dimensional along the stem where the temperatures were measured (see Figs. 6 and 8). Thus, the magnitude of the heat flux could be determined directly from the temperature difference, i. e.,

$$\dot{Q} = KA \frac{dT}{dx} = \frac{K\pi d^2}{4} \frac{(T_1 - T_2)}{l}$$

The stem diameter, d , and the distance between thermocouples, l , were carefully measured during probe construction, and the conductivity, K , of high-purity copper was taken from Fig. 10 with the material temperature taken to be $(T_1 + T_2)/2$.

The next step in the data reduction procedure was to determine the heat flux to a completely cold-wall model ($T_w = 0^\circ R$). This was done by estimating the actual wall temperature of the model (by extrapolating the known stem temperatures to the nose) and then increasing the measured heat flux by $1/(1 - T_w/T_0)$ which was approximately 1/0.85 for all models. This is the quantity plotted in Figs. 11 and 12 and also tabulated in Tables II and III. These figures and tables present the measured results of the test, adjusted to the cold-wall condition. In each case Q represents the total heating rate to all portions of the model forward of the station for which Q is given.

In this report comparisons of the data with earlier theories and data involve making use of the heat flux distributions around simple axisymmetric bodies given in Ref. 4 for a hypersonic, continuum flow.

For the first model (spherical nose segment) it was assumed that the distribution given by Lees was valid. Thus,

$$\dot{Q} = \dot{q}_0 \int_0^{A_{rea}} \dot{q}/\dot{q}_0 dA$$

or

$$\frac{\dot{Q}}{\dot{q}_0 2\pi R_n^2} = \int_0^{80^\circ} \dot{q}/\dot{q}_0 \sin \theta d\theta$$

The right-hand side can be found from Ref. 4 and is shown in Fig. 13. Because \dot{Q} is the quantity measured, a value for the stagnation point heat flux, \dot{q}_0 , can be found. This is nondimensionalized by a computed value of \dot{q}_{0f-r} (Ref. 5) and then compared with previously obtained data and several theories in Fig. 14. The agreement is satisfactory.

This quantity, \dot{q}_0 , is also used in Figs. 15 and 16, where $\dot{Q}/\dot{q}_0 2\pi R_n^2$ is plotted as a function of distance along the body. This yields the discrete points. The broken lines connecting the points represent an attempt to show the most probable distribution of body heating rate.

These tentative distributions were obtained by first assuming that Lees' distribution (as shown in Fig. 17) is valid for the spherical segment-cone portion. This forces the curve to pass through zero at $x/L = 0$ and through the first data point (the second point plotted), so that agreement with the second data point (third point plotted) is the only experimental check on the assumed distribution. As shown in Figs. 15 and 16, this agreement is good.

To find an approximate distribution between the second and third data points, it was assumed that the flow past the 20-deg cone section was similar to the flow past a hypothetical, spherically capped 20-deg cone frustum as given by Fig. 17. The actual physical distance along the surface of the cone between the two data points was retained, but the theoretically based broken curve was forced to pass through the third data point. Again, the agreement between the second data point and the broken line is the only criterion for the validity of the assumed distribution. The degree of agreement may be assessed by inspecting Figs. 15 and 16.

For the distribution along the cylindrical portion, the distribution was assumed to vary as $\dot{q}/\dot{q}_0 = C\sqrt{x/L}$ (the flat-plate law), with the constant chosen to force agreement at both the third and fourth data points.

It should be emphasized that the distribution of heat flux depicted by the broken lines on Figs. 15 and 16, although it appears tenable, is

not necessarily valid and was not measured. This, however, in no way invalidates the points, shown in the same figures, which were measured.

In Fig. 18, the measured total heat flux to the disk without the shroud ($\alpha = 0$) is compared with previous data. Since the previous data represent measurements made on models with the sensing element diameter equal to the cylinder diameter, and since in the present case the sensing element diameter is slightly less than the nose diameter, this comparison (Fig. 18) is not entirely appropriate. Another difference in model configuration is that the present model has a 30-deg bevel on the rim (see Fig. 9). Both of these differences would tend to reduce heating rate to the present nose configuration, as shown qualitatively in Fig. 18.

It might be noted that the Teflon[®] insulation on this particular configuration ablated slightly during the acquisition of these data. This ablation slightly changed the configuration but should not have affected the reported data, since the products of ablation were swept away from the sensing surface.

SECTION IV CONCLUSIONS

Heat-transfer measurements have been made on a satellite-type model in a test environment which simulates an altitude of roughly 60 miles for a full-scale vehicle. The data obtained should prove useful as a check on theoretical calculations which attempt to predict heat-transfer distributions in this flow regime. The results agree quite well with previous data, where comparisons are available, i.e., for the hemispherical nose cap. Marked influence of flow rarefaction was found.

The measurements for the shrouded disk show that, for this configuration in the present test environment, the flow is not sufficiently rarefied for the concept of accommodation coefficient to be meaningfully applied. A shroud extension of one body diameter reduced the heating rate of the flat nose to approximately $1/8$ of the value for no shroud in these tests.

REFERENCES

1. Sims, William H. "Aerodynamic Tests of Four Bodies in Low-Density, Hypersonic Flow." AEDC-TR-65-157 (AD466167), Revised and Reprinted, November 1965.
2. U. S. Committee on Extension to the Standard Atmosphere. U. S. Standard Atmosphere, 1962. U. S. Government Printing Office, Washington, D. C., December 1962.
3. Jakob, Max, "Heat Transfer." Vol. I, John Wiley and Sons, Inc., New York, March 1958, p. 109.
4. Lees, L. "Laminar Heat Transfer Over Blunt-Nosed Bodies at Hypersonic Flight Speeds." Jet Propulsion, Vol. 26, No. 4, April 1956, pp. 259-269, 274.
5. Fay, J. A. and Riddell, F. R. "Theory of Stagnation Point Heat Transfer in Dissociated Air." Journal of the Aeronautical Sciences, Vol. 25, No. 2, February 1958, pp. 73-85, 121.
6. Probstein, Ronald F. and Kemp, Nelson H. "Viscous Aerodynamic Characteristics in Hypersonic Rarefied Gas Flow." Journal of the Aero/Space Sciences, Vol. 27, No. 3, March 1960, pp. 174-192, 218.
7. Van Dyke, M. "Second-Order Compressible Boundary-Layer Theory with Application to Blunt Bodies in Hypersonic Flow." OSR-TN-61-1270, July 1961.
8. Potter, J. Leith and Miller, J. T. "Total Heating Load on Blunt Axisymmetric Bodies in Low-Density Flow." AIAA Journal, Vol. 1, No. 2, February 1963.
9. Potter, J. Leith and Miller, John T. "Experimental Heat Transfer to Blunt Axisymmetric Bodies Near the Limit of Continuum Flow." AEDC-TDR-62-155 (AD281911), August 1962.
10. Cheng, H. K. "The Blunt-Body Problem in Hypersonic Flow at Low Reynolds Number." CAL AF-1285-A-10 (AD411433), June 1963.

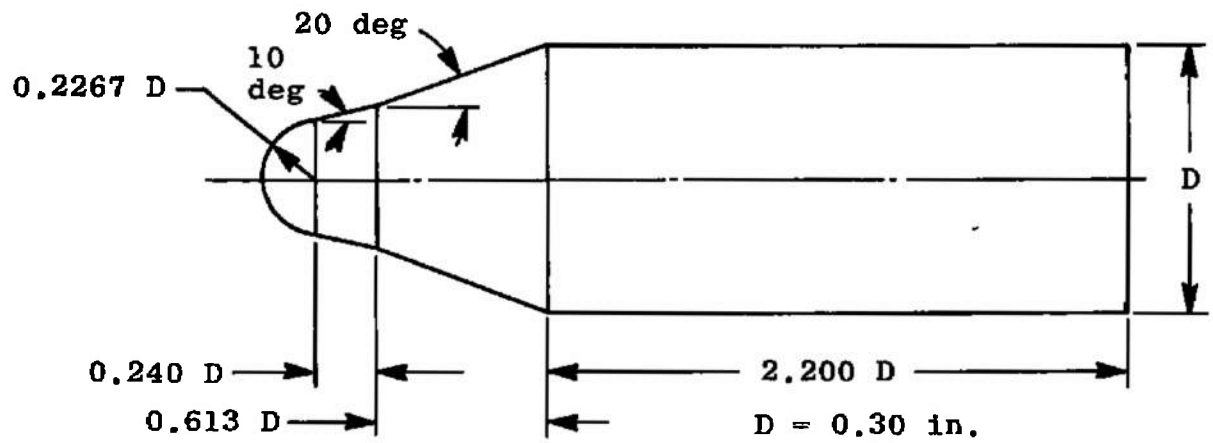


Fig. 1 Satellite Model

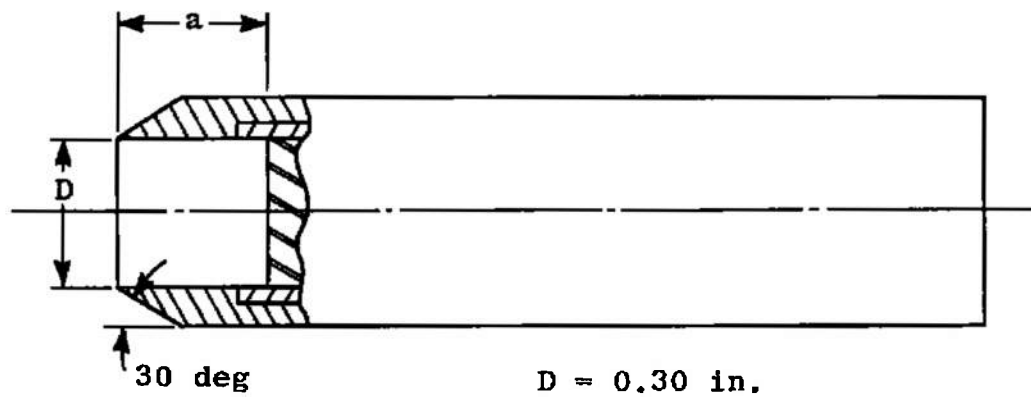


Fig. 2 Shrouded Disk



Fig. 3 Photograph of Test Models

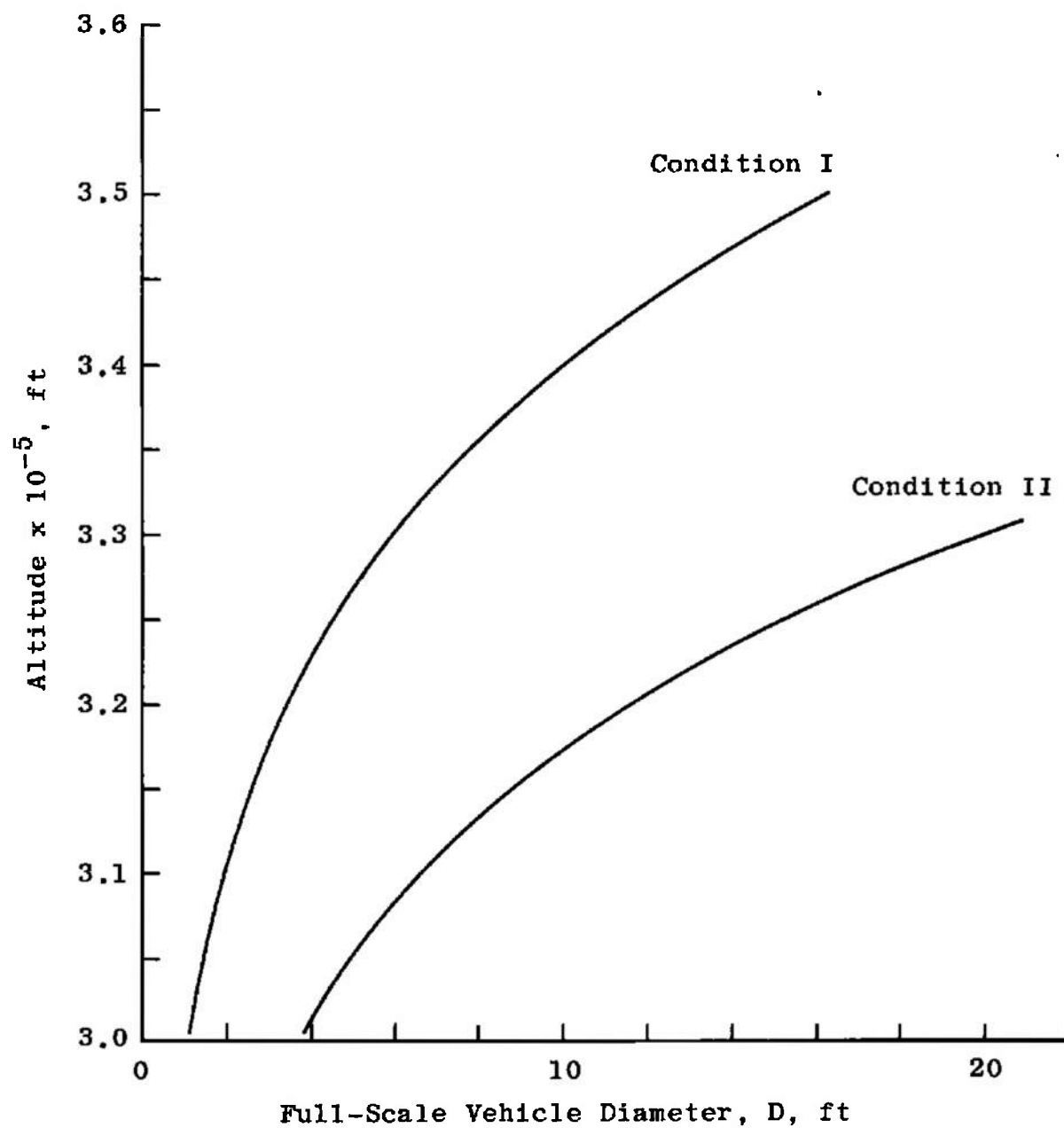


Fig. 4 Altitude versus Satellite Diameter for Knudsen Number Simulation

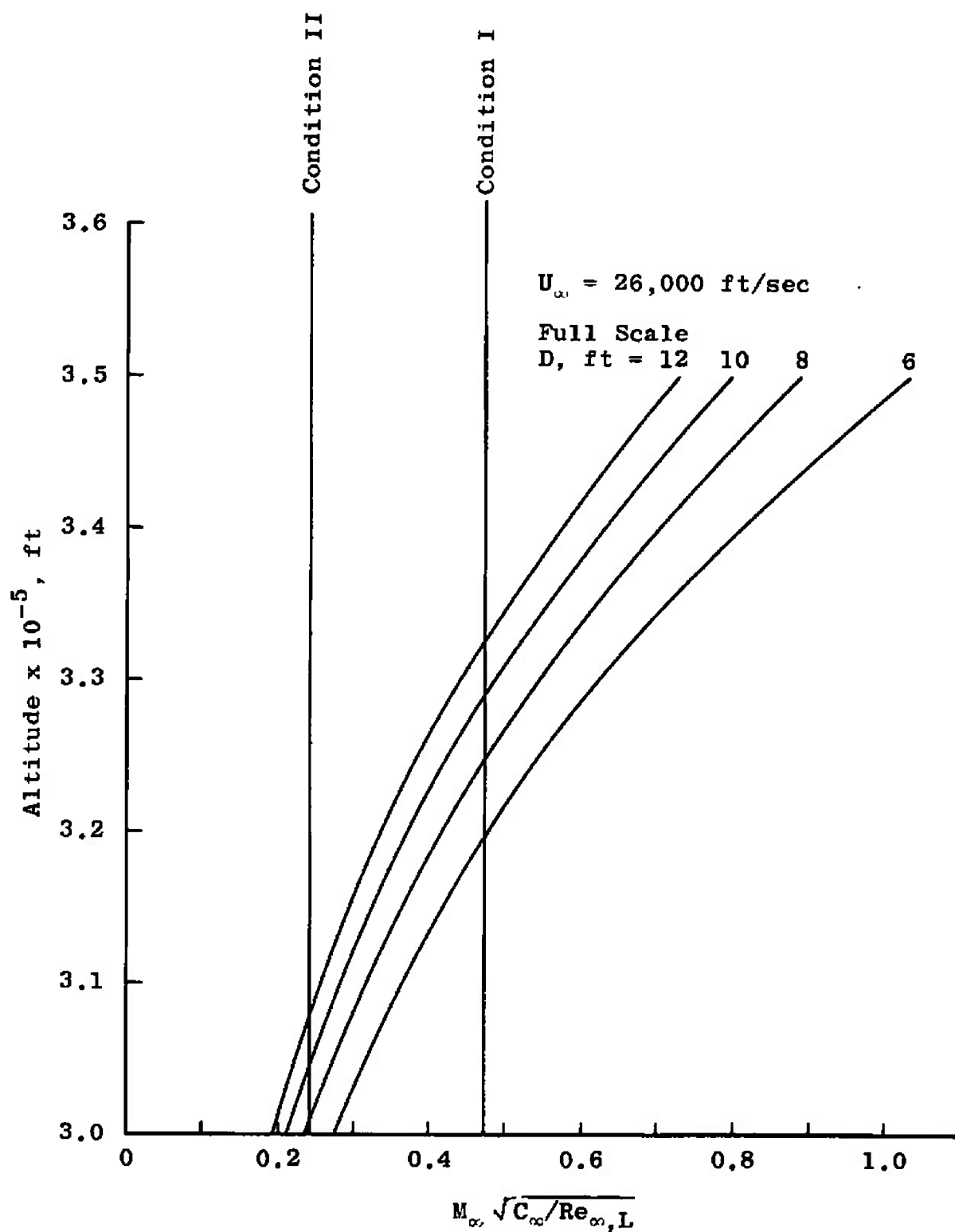


Fig. 5 Altitude versus Viscous Interaction Parameter for Various Satellite Diameters

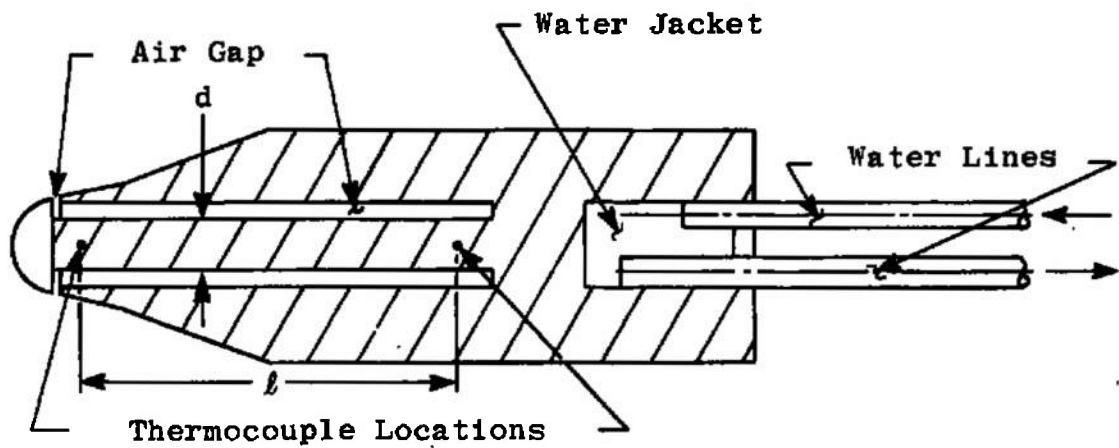


Fig. 6 Sketch of Model with Spherical Cap Forebody

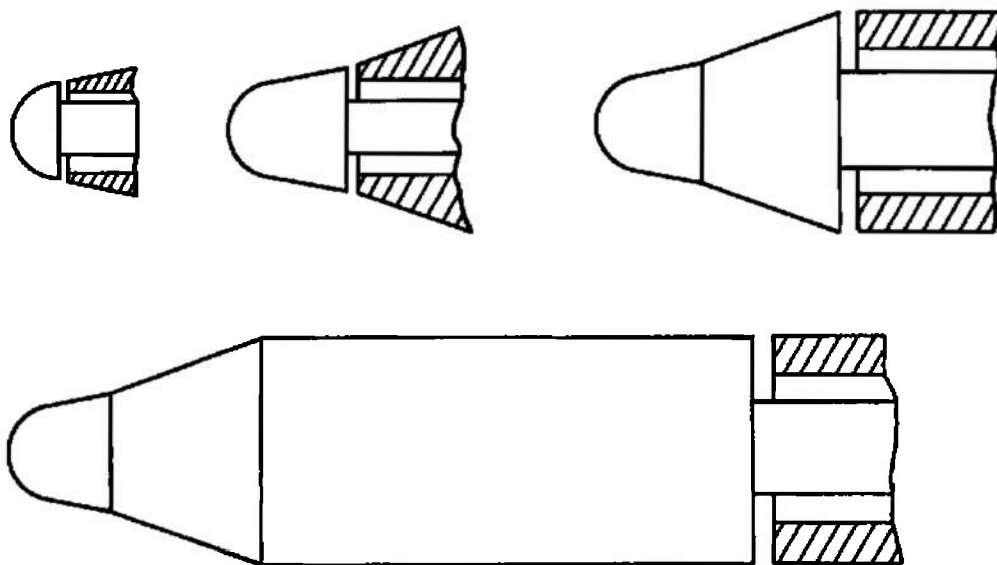
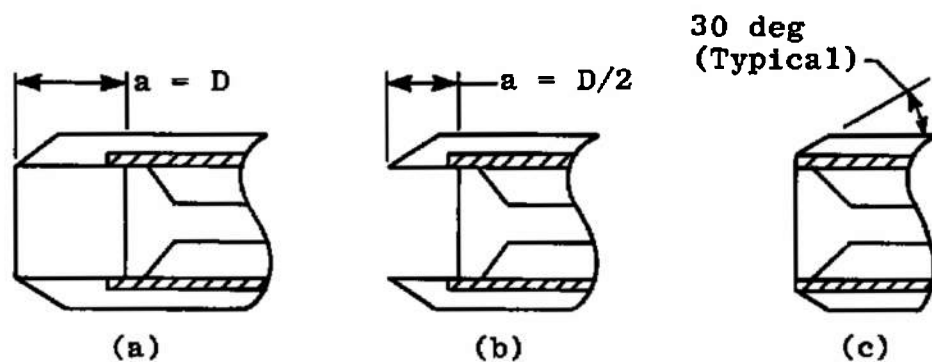
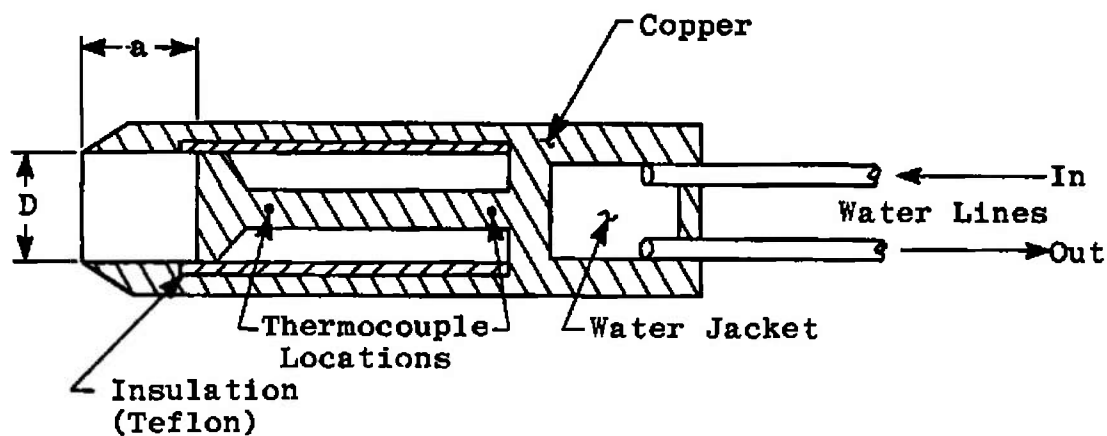


Fig. 7 Forebodies Used to Obtain Segments of Total Heating Distribution



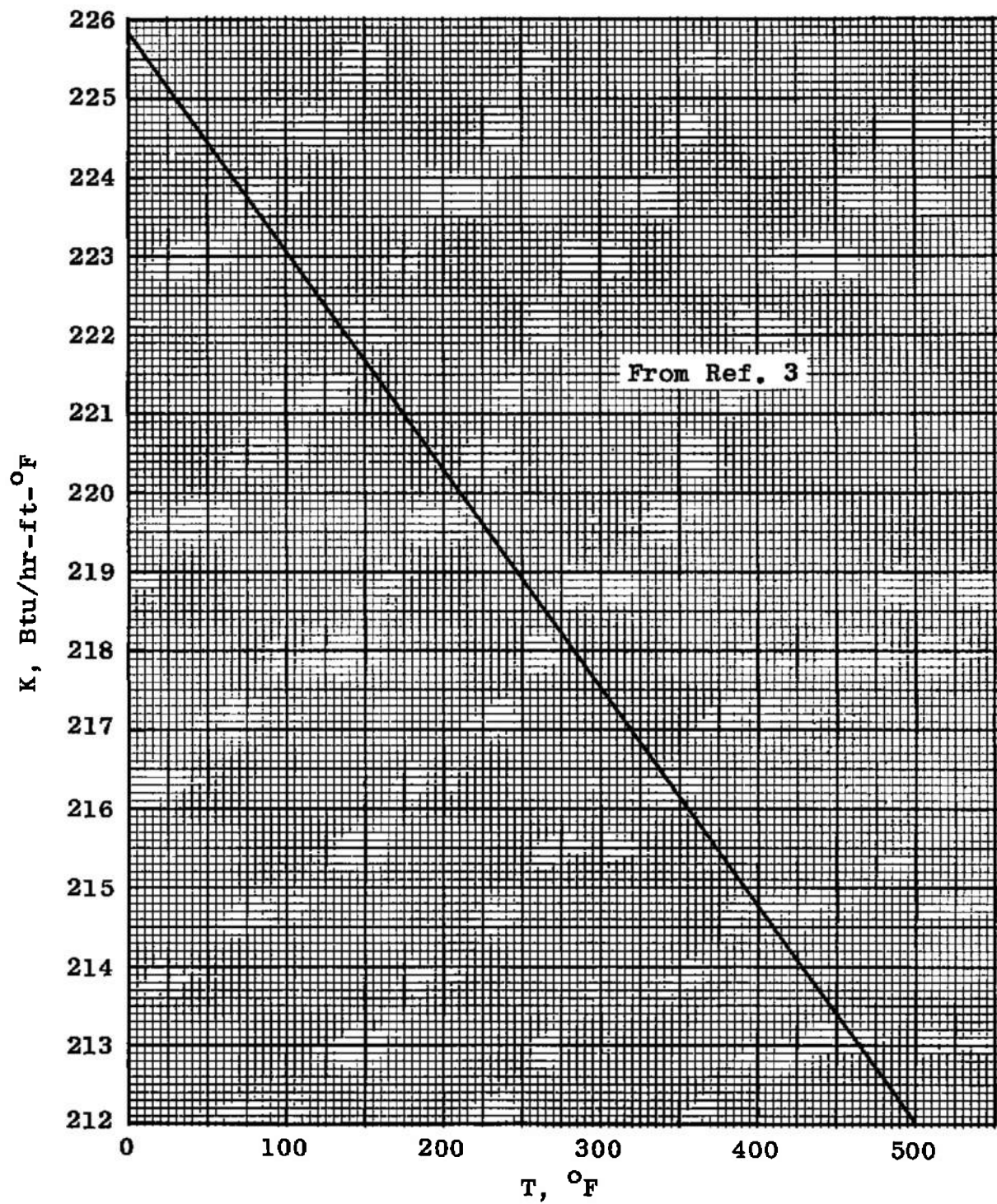


Fig. 10 Thermal Conductivity of Copper

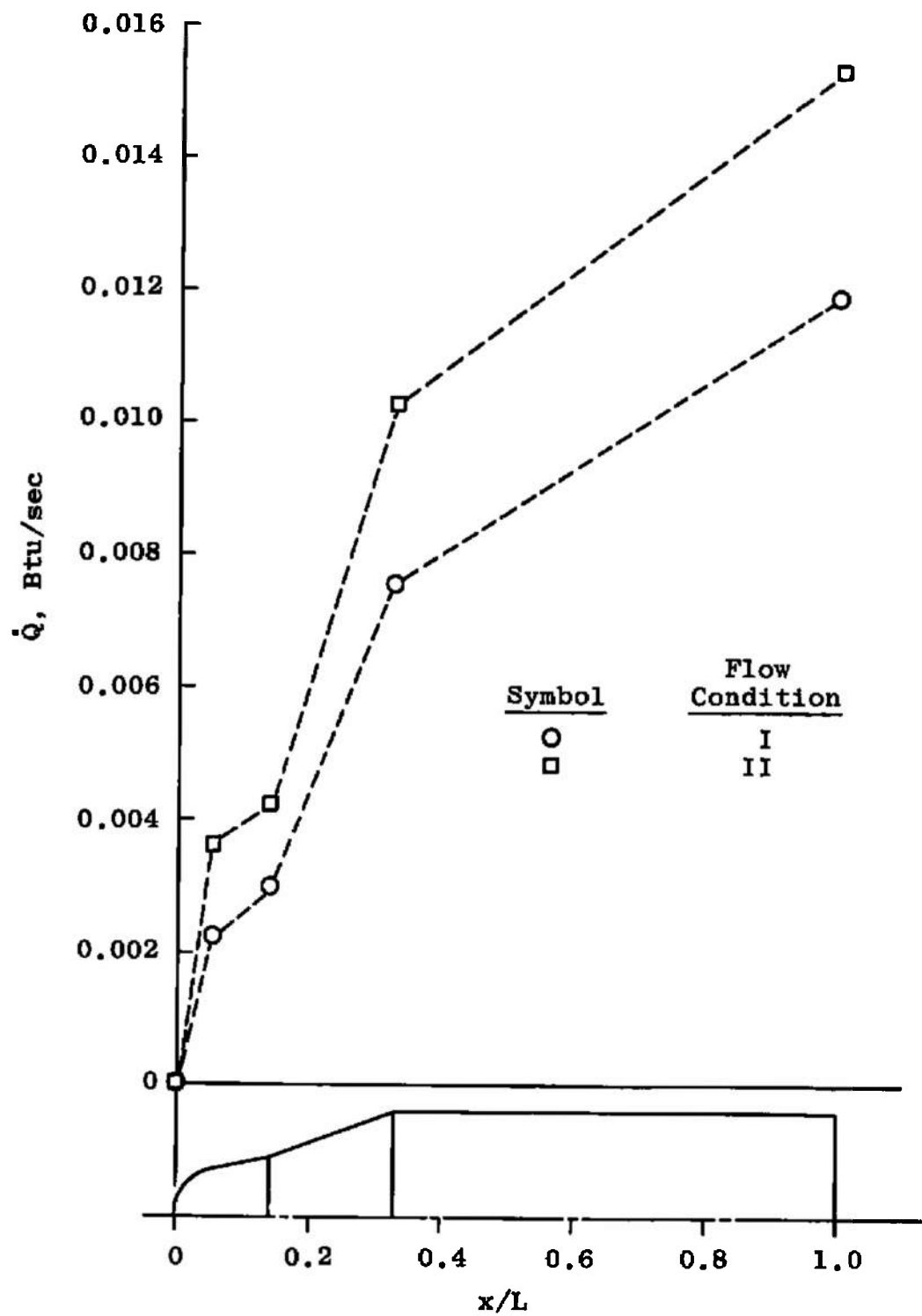


Fig. 11 Measured Heat Flux Referenced to Cold Wall

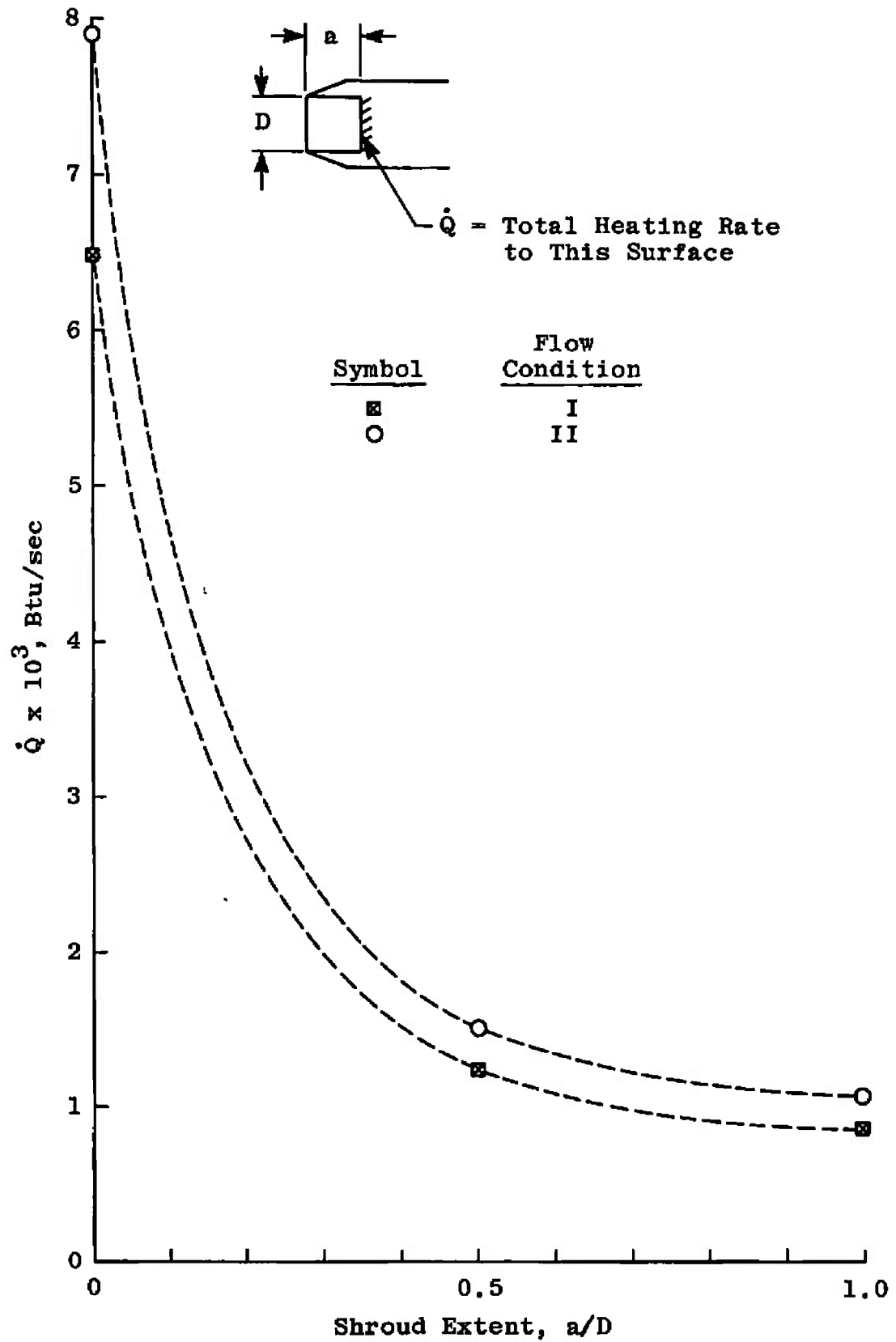


Fig. 12 Measured Heat Flux to Shrouded Disk Referenced to Cold Wall

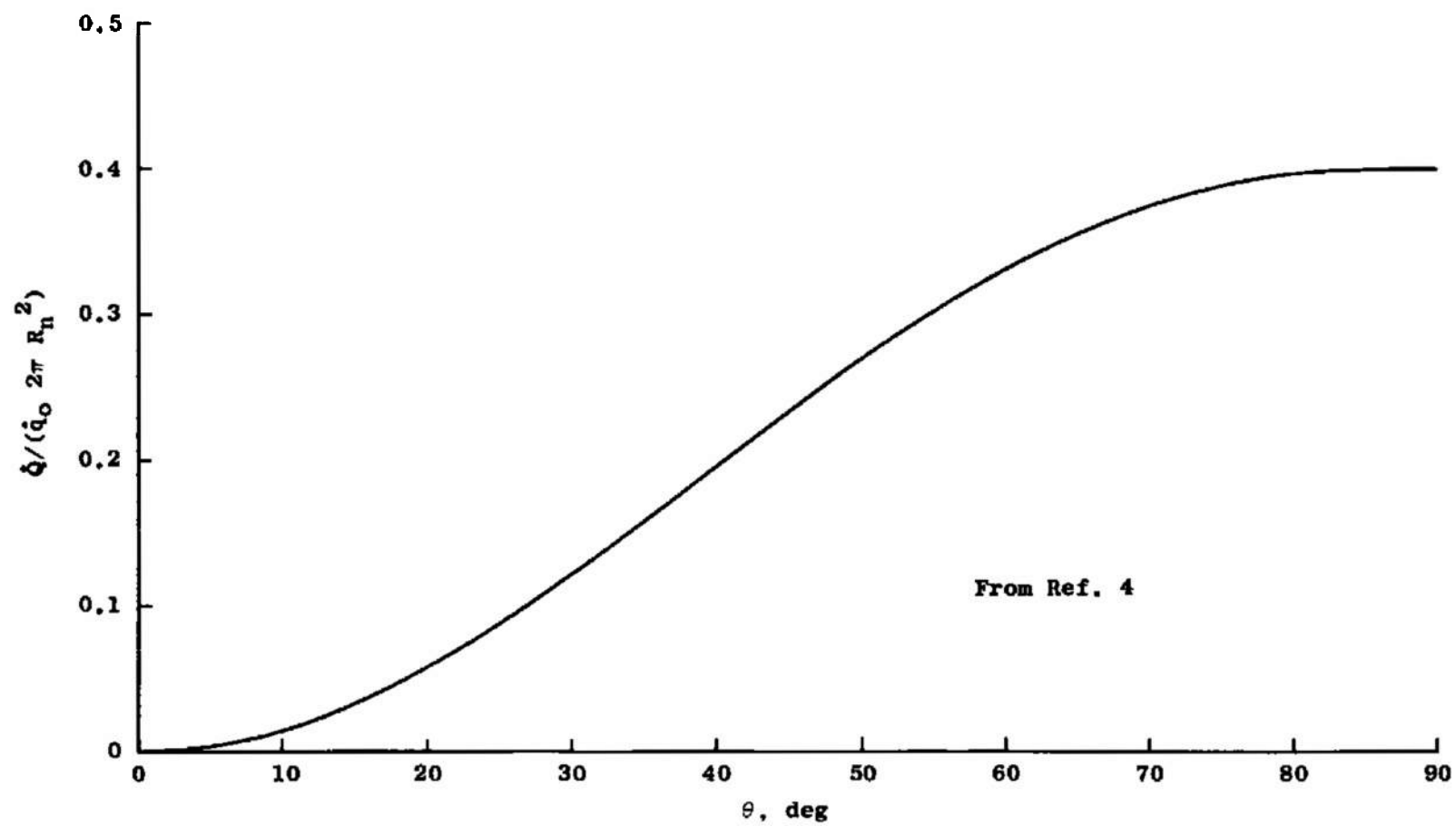


Fig. 13 Total Heating Rate to a Spherical Segment

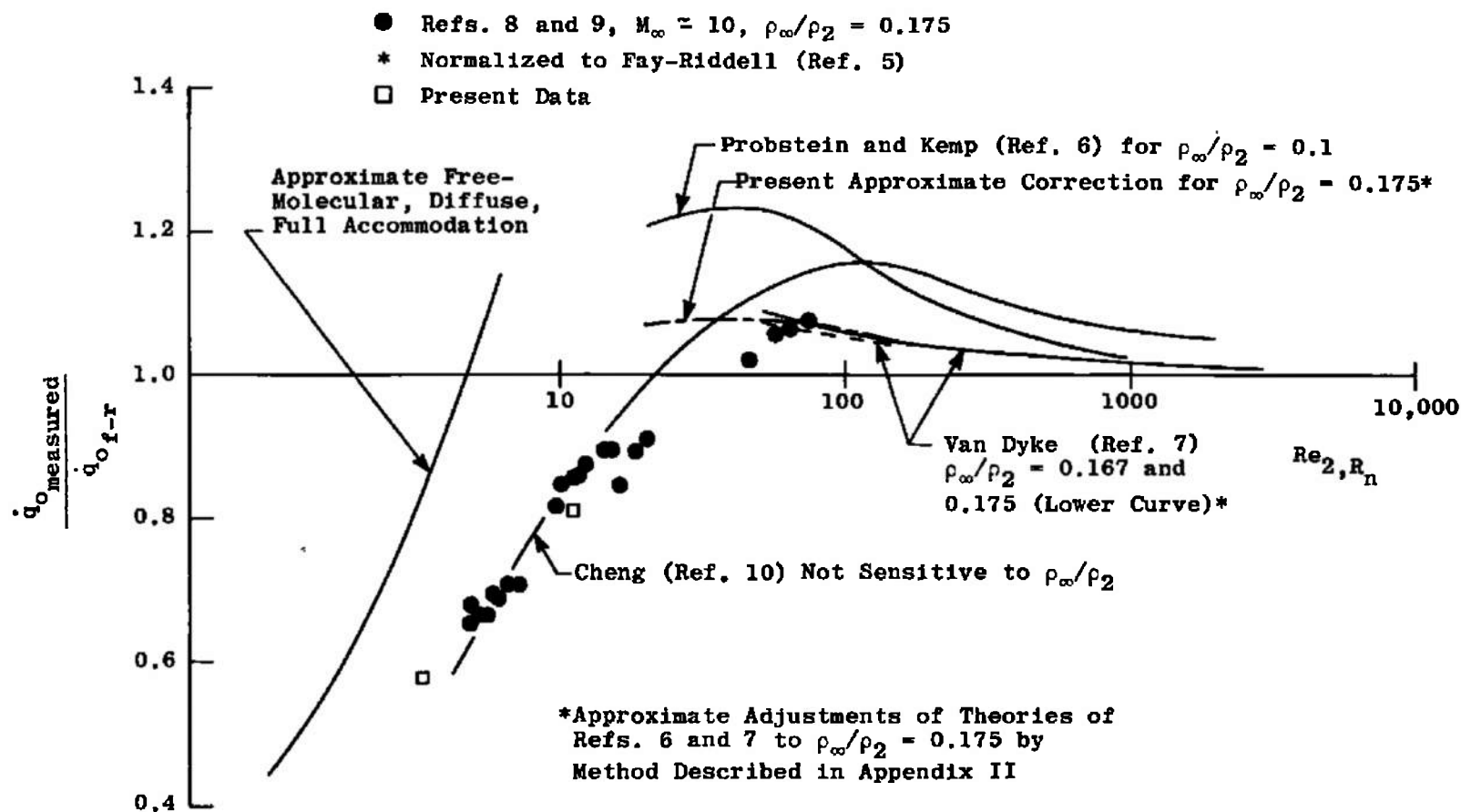


Fig. 14 Comparison of Present Data with Previous Data and Theories

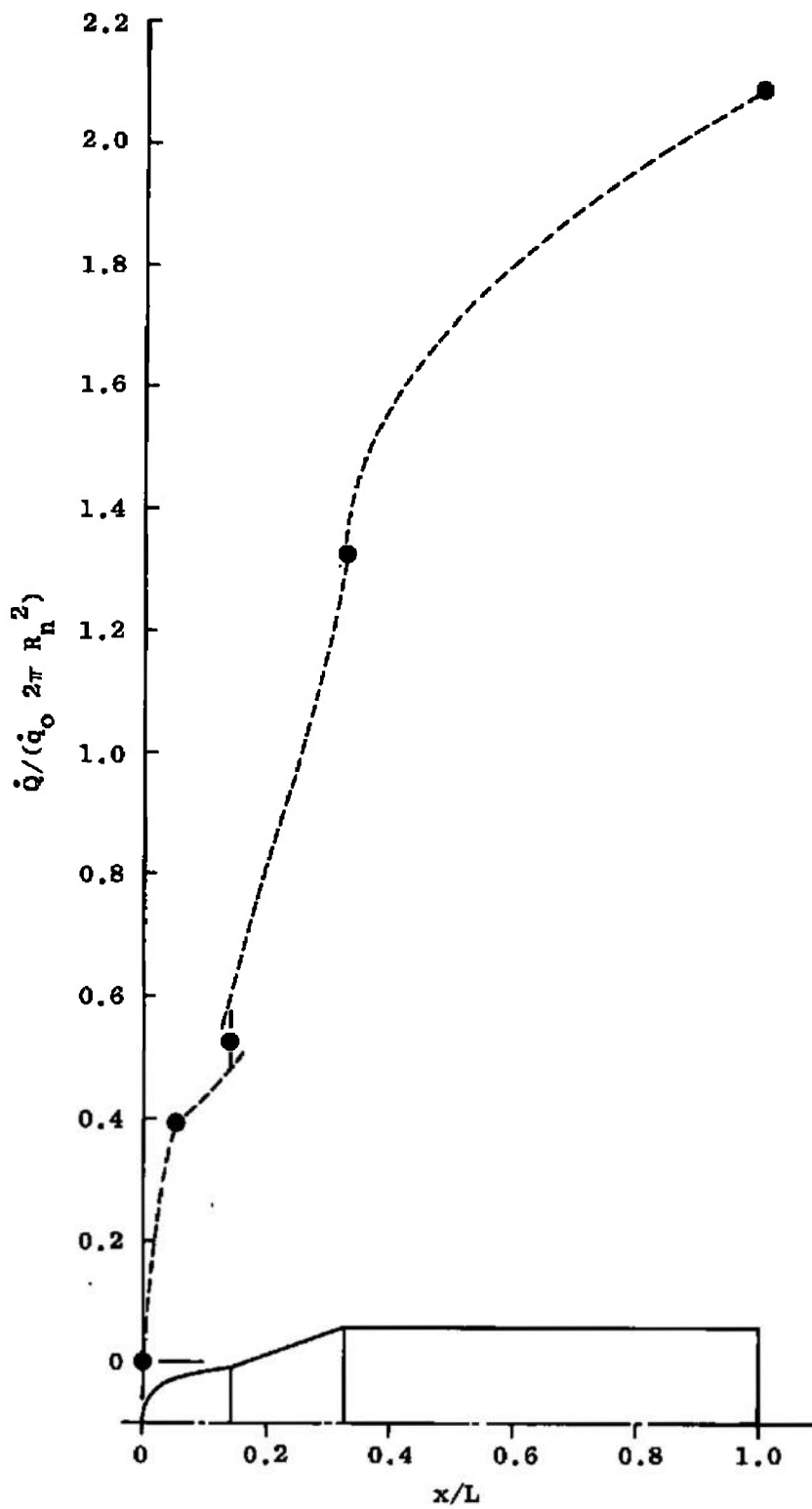


Fig. 15 Distribution of Heating Rate to Satellite Model: Condition I

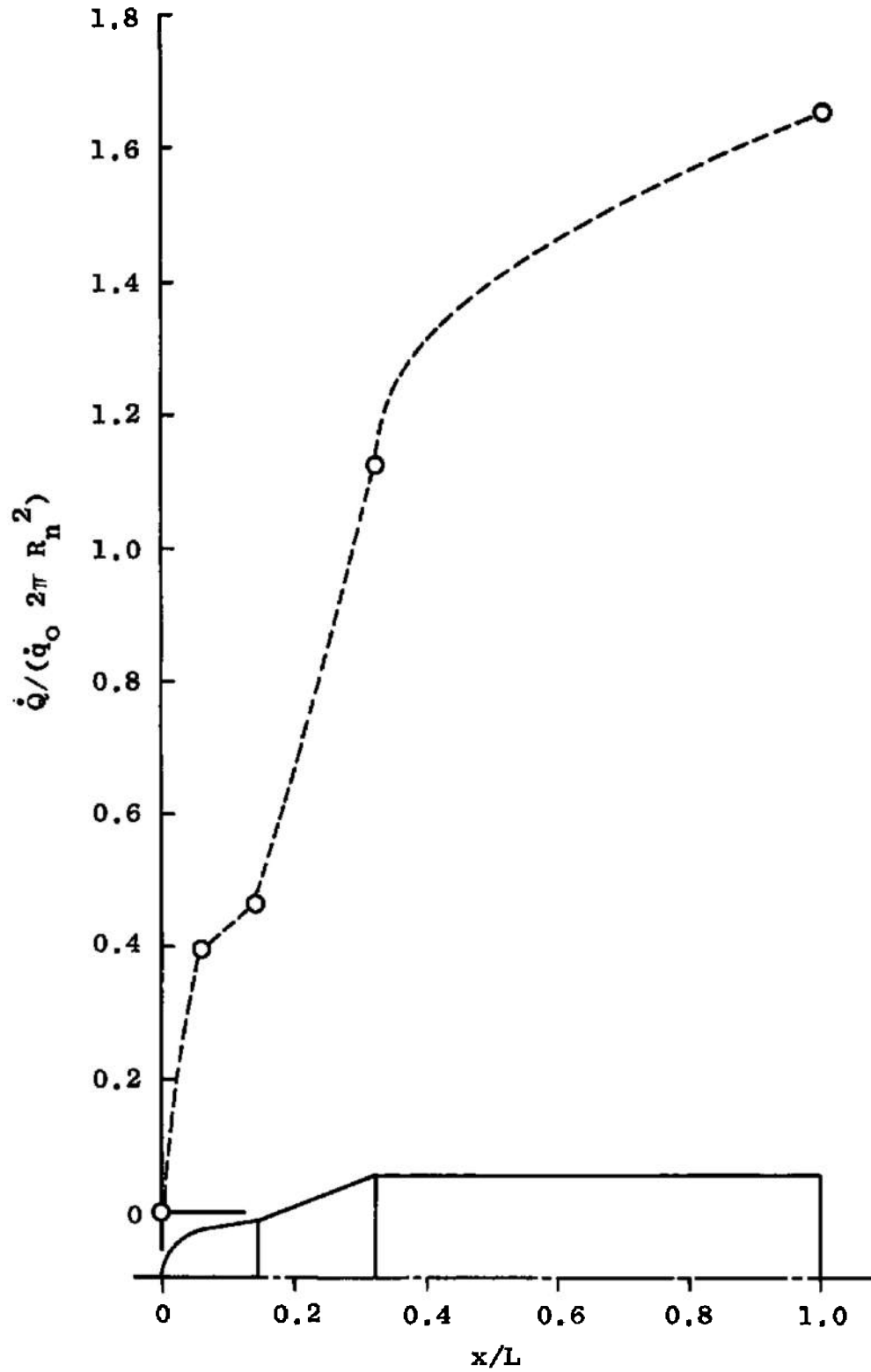


Fig. 16 Distribution of Heating Rate to Satellite Model: Condition II

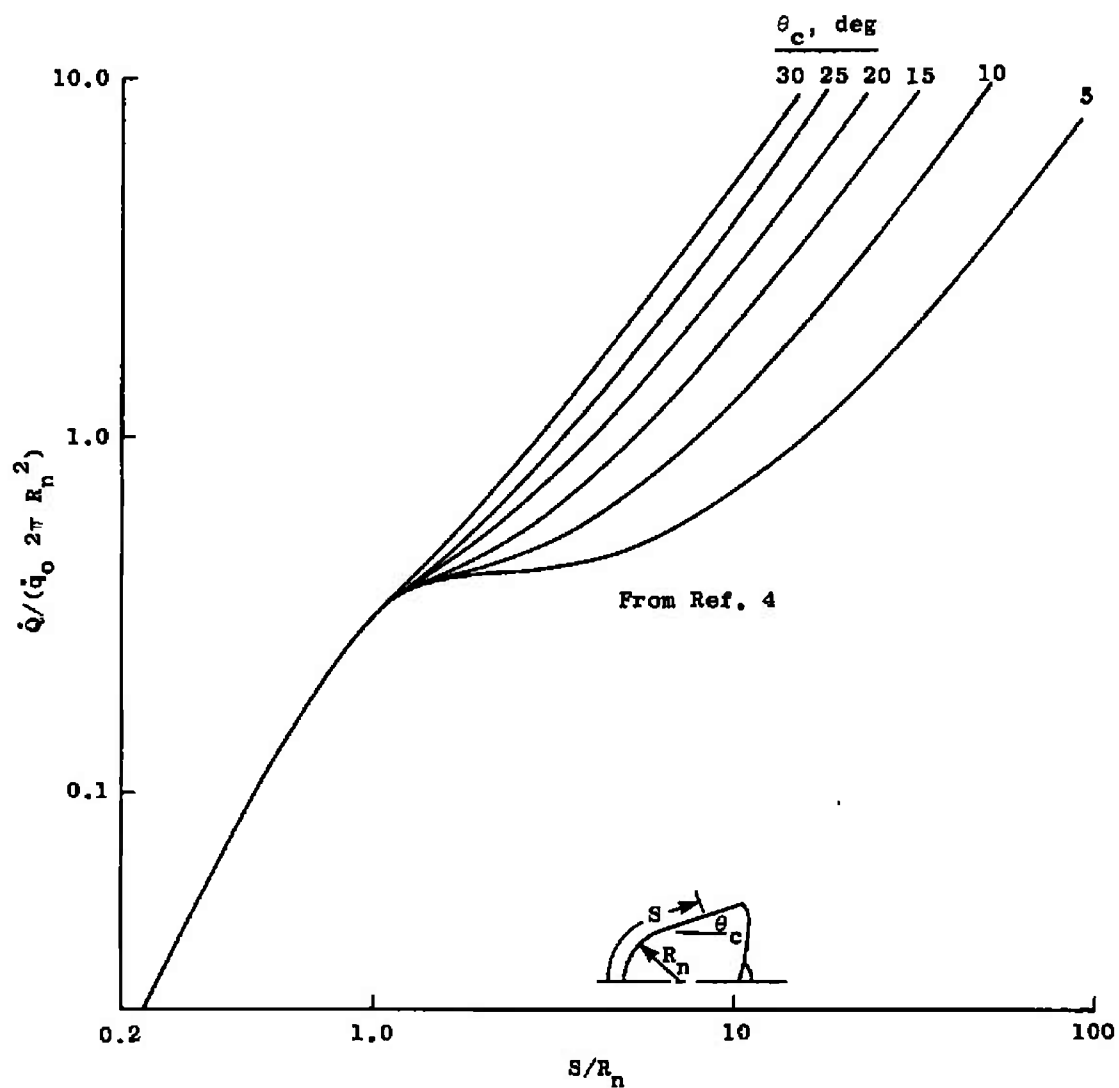


Fig. 17 Total Heating Rate to a Spherically Blunted Cone

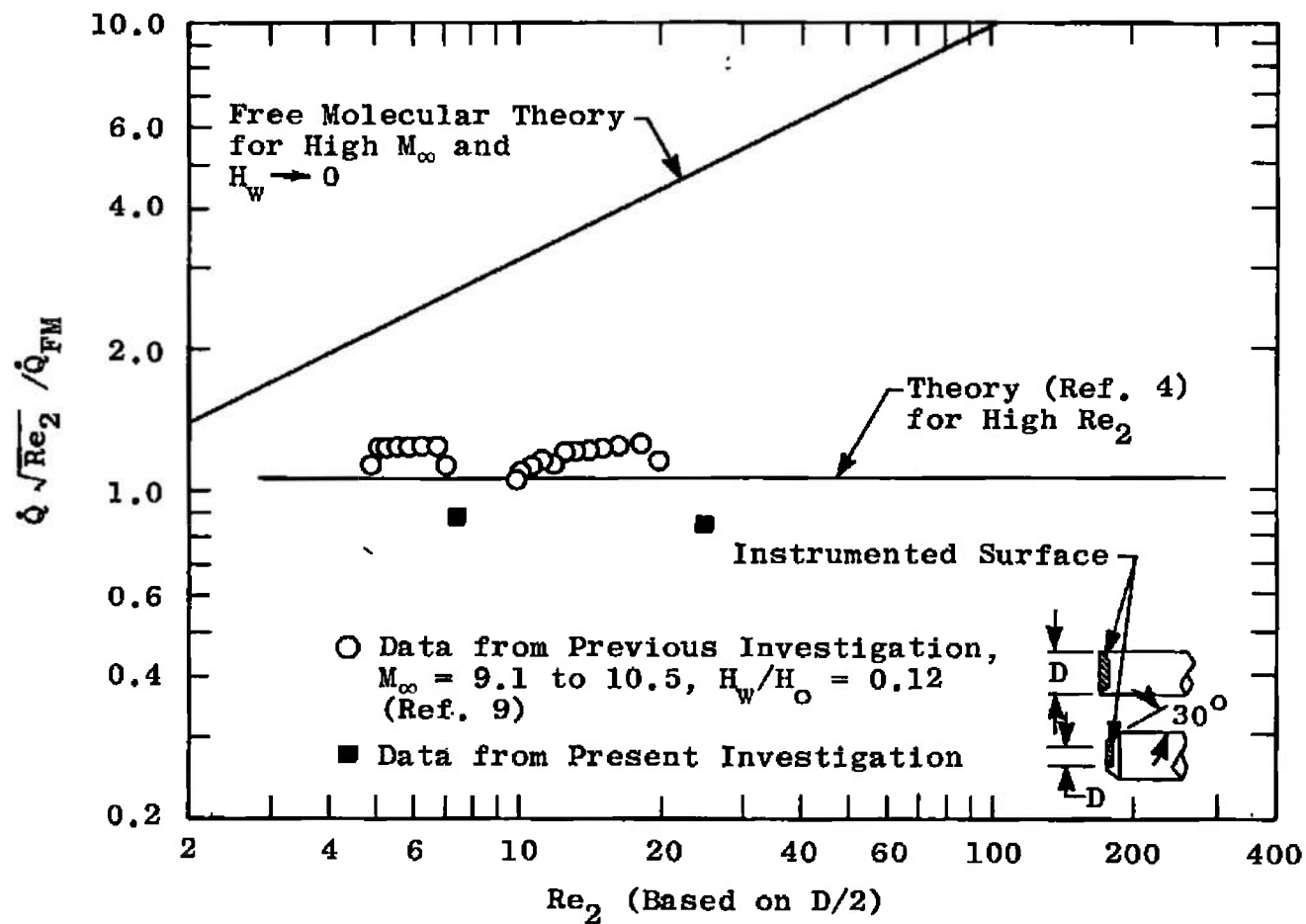


Fig. 18 Heat-Transfer Rate to a Flat Nose

TABLE I
TEST CONDITIONS

<u>Parameter</u>	<u>Condition</u>		<u>Units</u>
	<u>I</u>	<u>II</u>	
ρ_{∞}	3.84×10^{-6}	1.27×10^{-5}	lb _m /ft ³
T_{∞}	144.4	135	°K
p_{∞}	20.5	60.5	μHg
$Re_{\infty}/in.$	388	1200	in. ⁻¹
U_{∞}	8117	7225	ft/sec
q_{∞}	3.98	10.3	lb _f /ft ²
M_{∞}	10.15	9.3	
T_o	3122	2365	°K
p_o	18.0	30.0	lb _f /in. ²
p_o'	2620	6840	μHg
λ_{∞}	0.0395	0.0117	in.
$Re_2/in.$	49.7	166.3	in. ⁻¹
H_o	1625	1198	Btu/lb _m
\dot{q}_{of-r}	48.5	56.6	Btu/sec-ft ²

TABLE II
MEASURED VALUES OF HEATING RATE TO SEGMENTS OF SATELLITE VEHICLE,
REFERENCED TO COLD WALL

<u>Model</u>	<u>\dot{Q}, Btu/sec</u>	
	<u>Condition I</u>	<u>Condition II</u>
Spherical Nose Cap	0.00226	0.00364
Sphere-Cone	0.00299	0.00422
Sphere-Cone-Cone	0.00755	0.01026
Complete Configuration	0.01192	0.01539

TABLE III
MEASURED VALUES OF HEATING RATE TO SHROUDED DISK,
REFERENCED TO COLD WALL

<u>Shroud Length, a</u>	<u>\dot{Q}, Btu/sec</u>	
	<u>Condition I</u>	<u>Condition II</u>
D	0.00087	0.00108
D/2	0.00125	0.00150
0	0.00648	0.00789

APPENDIX I

TUNNEL L

TUNNEL DESCRIPTION

Tunnel L, shown in Fig. I-1, is a low density, hypersonic, continuous-type, arc-heated, ejector-pumped facility, normally using nitrogen or argon as the test gas and consisting of the following major components, in streamwise order:

1. Continuous, water-cooled, d-c arc heater, Thermal Dynamics Corporation Model F-40 or U-50, both modified slightly, with a 40-kw selenium rectifier power supply. Gas is injected without swirl in the F-40 arc heater and with or without swirl in the U-50 unit. Unless otherwise noted, all testing is done without use of swirling gas injection.
2. Cylindrical, water-cooled settling section of variable size, but normally of 3-in. diameter and 6- to 10-in. length.
3. Axisymmetric, aerodynamic nozzle, variable sizes with 0.10- to 1.20-in. -diam throats and 2.0- to 8.2-in. -diam exits. Three contoured nozzles having no flow gradients in the test section are currently available, in addition to older conical nozzles. Table I-1 gives the major characteristics of the contoured nozzles.
4. Cylindrical test section tank of 48-in. diameter surrounding the test section and containing instrumentation, cooling water connections, and probe carrier.
5. Axisymmetric diffuser with interchangeable designs for varying test conditions, convergent entrance, constant-area throat, divergent exit sections, and water-cooled entrance.
6. Water-cooled heat exchanger.
7. Isolation valve.
8. Air ejector of two stages.
9. Connection to the VKF evacuated, 200,000-cu-ft, spherical vacuum reservoir and its pumping system.

All critical components of the tunnel and related systems are protected by back-side water cooling. The two-stage ejector system is driven by air instead of steam because of the ready availability of high pressure air at the tunnel site. Although the working gas is normally

nitrogen or argon, other gases may be used. Typical ranges of operation with heated flow are given in Table I-2, and unheated-flow operational ranges are given in Table I-3. The first published description of this tunnel appeared in Ref. I-1.

TUNNEL INSTRUMENTATION AND CALIBRATION

Gas flow rate to the arc heater is measured through use of calibrated sonic-flow orifices, and reservoir pressure is measured with a Consolidated Electrodynamics Corporation Electromanometer®. Inaccuracy of these systems, on the basis of comparison with other means of measurement, and repeatability, is estimated to be less than ± 0.5 percent for both flow rate and reservoir pressure.

Total enthalpy at the nozzle throat is determined by use of a calorimeter which, on the basis of comparison of results and repeatability, appears accurate to within ± 4 percent limits of error. This measurement is supplemented by a probe system which measures local total enthalpy and mass flux in the test section with an estimated error limit of ± 2 percent for mass flux and ± 5 percent for enthalpy.

Impact pressures are measured with variable reluctance, differential pressure transducers and water-cooled probes. Calibration of the transducers is accomplished by means of an oil-filled micro-manometer and a McLeod gage. Inaccuracy in impact pressure measurement is believed not to exceed ± 2 percent limits. Static pressures are measured by the same method, but are not used for primary calibration purposes because of the very large corrections for viscous and rarefied flow phenomena.

The establishment of reservoir conditions, determination of impact pressures, and proof of inviscid, adiabatic core flow through the nozzles form part of the flow calibration. This information is used in a calculation which accounts for nonequilibrium expansion of the gas throughout the nozzle to yield the needed flow properties. References I-2 through I-7 contain information on various aspects of these measurements.

A three-component balance is used for measuring lift, drag, and pitching moment on aerodynamic bodies in Tunnel L. This is described in Ref. I-8.

TABLE I-1
MAJOR CHARACTERISTICS OF TUNNEL L CONTOURED NOZZLES

	<u>Lower Reynolds No.</u>	<u>Higher Reynolds No.</u>	<u>Cold Flow</u>
Total Pressure, psia	18.0	30.0	0.235
Total temperature, °R	5400	4500	530
Mass Flow Rate, lb _m /hr	7.76	14.2	22
Throat Diameter, in.	0.1481	0.1469	1.2226
Exit Diameter, in.	8.160	4.814	5.494
Test Section Core Diameter, in.	1.5	2.0	3.2
Test Section M _∞	10.15	9.3	4.05
Test Section Unit Reynolds No. /in.	388	1200	1760

TABLE I-2
TUNNEL L OPERATING CONDITIONS WITH ARC HEATER

	<u>Nitrogen</u>	<u>Argon</u>
Total Pressure, psia	7.0 to 30.0	0.5 to 6.4
Total enthalpy, Btu/lbm	740 to 2130	280 to 960
Total Temperature, °R	2300 to 7200	2300 to 7700
Mach Number	4.8 to 10.8	3.7 to 16.1
Unit Reynolds Number, Free Stream, in. ⁻¹	300 to 3500	270 to 4700
Unit Reynolds Number behind Normal Shock, in. ⁻¹	35 to 1140	14 to 1080
Mean Free Path, Free-Stream, Static Billiard-Ball Gas Model, in.	0.002 to 0.058	0.002 to 0.057
Uniform Flow Core Diameter at Test Section, in.	0.2 to 2.0	0.5 to 1.5

TABLE I-3
TUNNEL L OPERATING CONDITIONS WITHOUT ARC HEATER

	<u>Nitrogen</u>	<u>Argon</u>
Total Pressure, psia	0.06 to 2.7	0.08 to 3.0
Total Enthalpy, Btu/lb	140	70
Total Temperature, °R	530	530
Mach Number	3.8 to 5.8	4.0 to 8.0
Unit Reynolds Number Free Stream, in. ⁻¹	620 to 15,000	1600 to 50,000
Unit Reynolds Number behind Normal Shock, in. ⁻¹	190 to 3500	264 to 3800
Mean Free Path, Free-Stream, Static Billiard-Ball Gas Model, in.	0.0005 to 0.012	0.0001 to 0.006
Uniform Flow Core Diameter at Test Section, in.	0.8 to 3.2	0.5 to 1.0

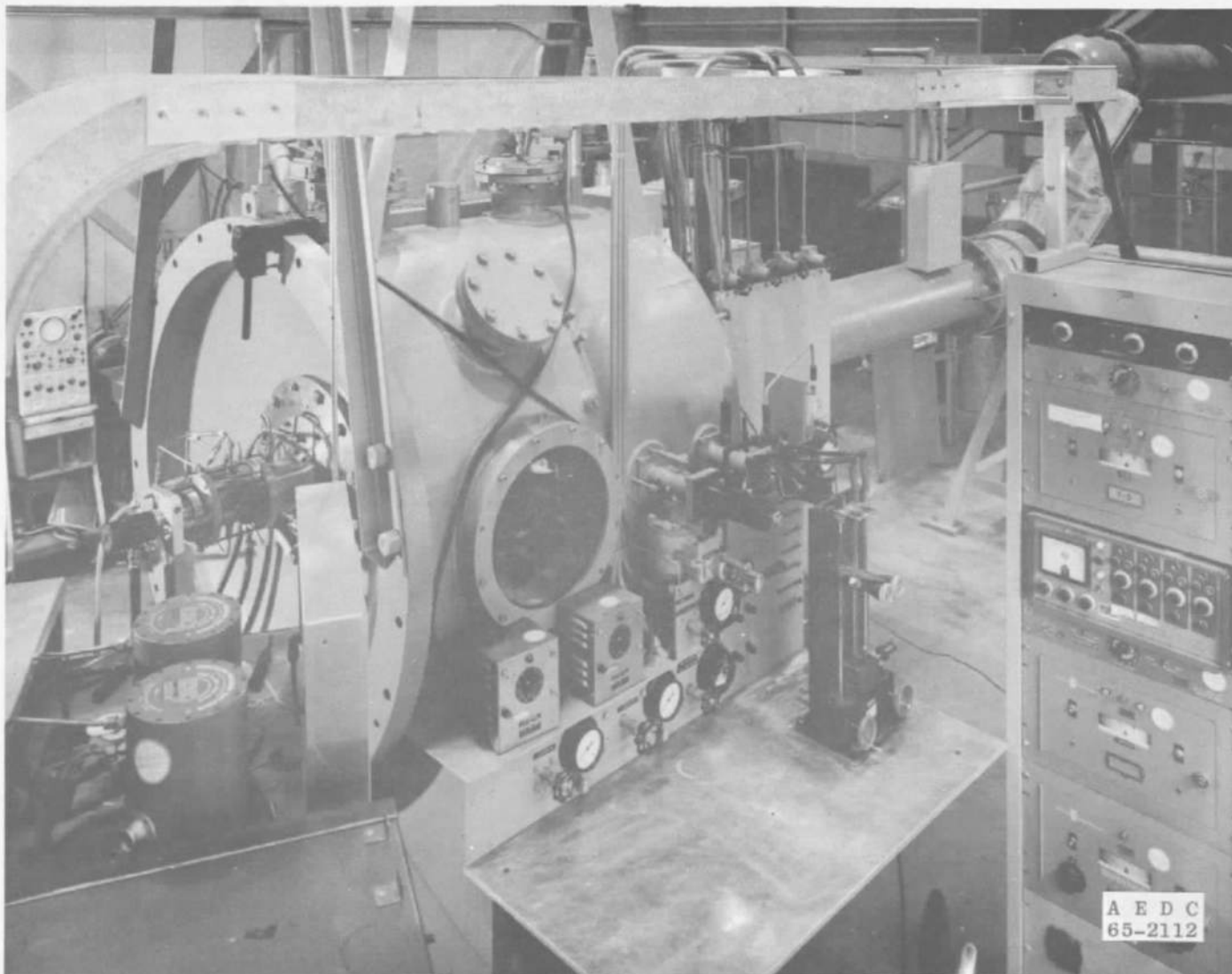


Fig. 1-1 Low Density Hypersonic Wind Tunnel L (January 1966)

APPENDIX II

EFFECT OF DENSITY RATIO ON SECOND-ORDER STAGNATION REGION HEATING RATE AND SKIN FRICTION

By
J. Leith Potter

Various authors (e.g., Refs. II-1 through II-4) have published results of analyses giving blunt-body stagnation region heating rate and skin friction under rarefied hypersonic flow conditions. Usually the numerical results are presented for some specific shock-crossing density ratio, ϵ , where

$$\epsilon = \rho_{\infty} / \rho_2$$

and it is difficult to determine what the ratios \dot{q} / \dot{q}_{BL} or τ / τ_{BL} would be if calculated for different values of ϵ . * This note is appended to give a description of a method devised to enable quick conversions from given numerical results for one value of ϵ to results for another ϵ . It must be emphasized that this conversion assumes constant values of Re_2 and T_w / T_0 in the conversion, and it further assumes the same hypersonic blunt body (strong-shock) approximations used in the basic analyses referenced.

Considering that the result of Probstein and Kemp (Ref. II-1), or similar results, can be expressed as

$$(\dot{q} - \dot{q}_{BL}) / \dot{q}_{BL} = k_1 \Omega - k_2 \Omega^2 + \dots$$

it follows that

$$(\dot{q} - \dot{q}_{BL})_1 / (\dot{q} - \dot{q}_{BL})_2 = \frac{\Omega_1}{\Omega_2} \left(\frac{1 - (k_2/k_1) \Omega_1}{1 - (k_2/k_1) \Omega_2} \right)$$

Then, to first order in Ω ,

$$(\dot{q} - \dot{q}_{BL})_1 / (\dot{q} - \dot{q}_{BL})_2 = \Omega_1 / \Omega_2 \quad (\text{II-1})$$

From Ho and Probstein (Ref. II-2),

$$\Omega = \frac{(1 - 8\epsilon/3)}{(2\epsilon)^{1/4} (8\epsilon/3)^{1/4}} \left(\frac{\rho_w \mu_w}{\rho_2 \mu_2} \right)^{1/2} \frac{(1 - \epsilon)^{1/2}}{Re_2^{1/2}} \quad (\text{II-2})$$

But

$$\left(\frac{\rho_w \mu_w}{\rho_2 \mu_2} \right)^{1/2} = \left(\frac{p_0}{p_2} \right)^{1/2} \left(\frac{T_2}{T_0} \frac{T_0}{T_w} \right)^{\frac{1-\omega}{2}}$$

*See nomenclature at end of appendix.

and, for $1.67 \geq \gamma \geq 1.2$, i. e., the range of interest here, with constant T_w/T_o , as specified in the beginning,

$$\left(\frac{\rho_w \mu_w}{\rho_2 \mu_2} \right)^{1/2} \approx \text{const.}$$

Hence, from Eqs. (II-1) and (II-2), with Re_2 also held constant,

$$(\dot{q} - \dot{q}_{BL})_1 / (\dot{q} - \dot{q}_{BL})_2 = \left(\frac{1 - 8\epsilon_1/3}{1 - 8\epsilon_2/3} \right) \left(\frac{\epsilon_2}{\epsilon_1} \right)^{5/4} \left(\frac{1 - \epsilon_1}{1 - \epsilon_2} \right)^{1/2} \quad (\text{II-3})$$

The quantity $(1 - 8\epsilon/3)(1 - \epsilon)^{1/2}/\epsilon^{5/4}$ is plotted in Fig. II-1 where, for example, it may be found that

$$(\dot{q} - \dot{q}_{BL})_{\epsilon=0.175} / (\dot{q} - \dot{q}_{BL})_{\epsilon=0.100} = 0.35$$

It is interesting to note that Van Dyke (Ref. II-3) found the influence of vorticity to vary as $\epsilon^{-5/4}$, curvature as $\epsilon^{-3/4}$ and slip and temperature jump as $\epsilon^{1/4}$. The present result, for $0.075 \leq \epsilon \leq 0.25$ is approximately $\Omega \sim \epsilon^{-5/2}$.

In view of the nature of the correction, it seems suitable for application to the results given in any of the references. Also, while the heat-transfer rate has been considered in the foregoing development, the relation derived could be used for skin friction coefficients just as well.

APPENDIX II NOMENCLATURE

k	Constant
p_o'	Pressure at stagnation point on body
\dot{q}	Heat-transfer rate, Btu/ft ² -sec
Re_2	Reynolds number based on flow immediately behind assumed Rankine-Hugoniot normal shock wave and nose radius of curvature
T	Temperature
γ	Ratio of specific heats
ϵ	ρ_w / ρ_2
μ	Coefficient of viscosity

ρ	Mass density
τ	Skin friction, lb_f/ft^2
Ω	See Eq. (II-2)
ω	Exponent in the relation $\mu \sim T^\omega$

SUBSCRIPTS

2	Condition immediately behind Rankine-Hugoniot normal shock wave
BL	Results for thin boundary layer, i. e., high Reynolds numbers
o	Total or reservoir conditions
w	Condition on surface of body

REFERENCES

- II-1 Probstein, Ronald F. and Kemp, Nelson H. "Viscous Aerodynamic Characteristics in Hypersonic Rarefied Gas Flow." Journal of the Aero/Space Sciences, Vol. 27, No. 3, March 1960, pp. 174-192, 218.
- II-2 Ho, Hung-Ta and Probstein, Ronald F. "The Compressible Viscous Layer in Rarefied Hypersonic Flow." Rarefied Gas Dynamics. Academic Press, New York and London, 1961, pp. 525-552.
- II-3 Van Dyke, Milton. "Second-Order Compressible Boundary Layer Theory with Application to Blunt Bodies in Hypersonic Flow." Hypersonic Flow Research. Academic Press, New York and London, 1962, pp. 37-80.
- II-4 Cheng, H. K. "The Blunt-Body Problem in Hypersonic Flow at Low Reynolds Number." CAL AF-1285-A-10 (AD411433), June 1963.

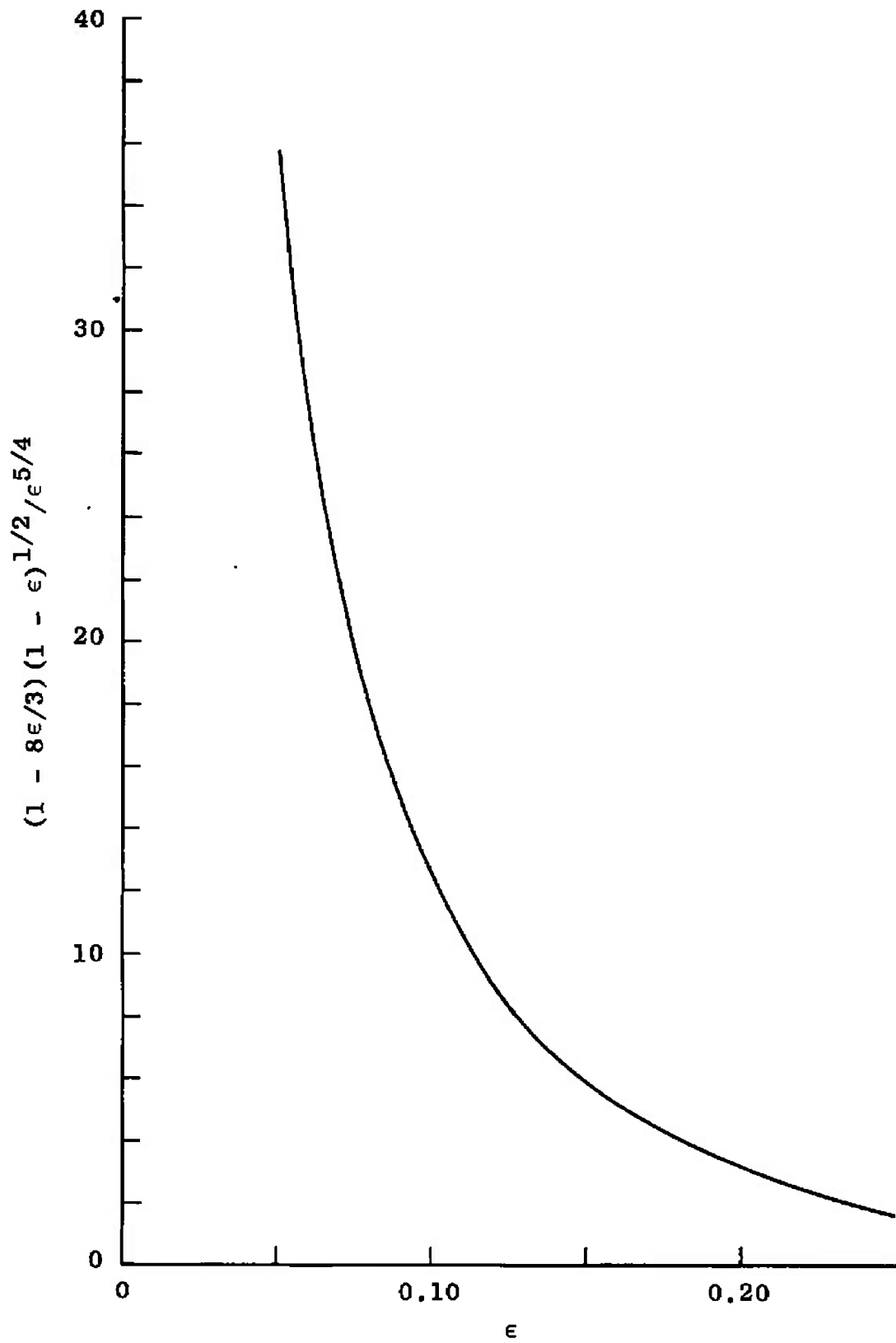


Fig. II-1 Function of Density Ratio

UNCLASSIFIED
Security Classification

DOCUMENT CONTROL DATA - R&D

(Security classification of title, body of abstract and indexing annotation must be entered when the overall report is classified)

1. ORIGINATING ACTIVITY (Corporate author) Arnold Engineering Development Center ARO, Inc., Operating Contractor Arnold AF Station, Tennessee		2a. REPORT SECURITY CLASSIFICATION UNCLASSIFIED	
		2b. GROUP N/A	
3. REPORT TITLE HEAT-TRANSFER MEASUREMENTS ON A SATELLITE CONFIGURATION AND SHROUDED DISK			
4. DESCRIPTIVE NOTES (Type of report and inclusive dates) N/A			
5. AUTHOR(S) (Last name, first name, initial) Miller, J. T., ARO, Inc.			
6. REPORT DATE March 1966		7a. TOTAL NO. OF PAGES 46	7b. NO. OF REFS 22
8a. CONTRACT OR GRANT NO. AF 40(600)-1200		9a. ORIGINATOR'S REPORT NUMBER(S) AEDC-TR-66-40	
b. PROJECT NAME Program Element 65402234		9b. OTHER REPORT NO(S) (Any other numbers that may be assigned this report) N/A	
c.			
d.			
10. AVAILABILITY/LIMITATION NOTICES Qualified users may obtain copies of this report from DDC. Release to foreign governments or foreign nationals must have prior approval of AEDC (AETI).			
11. SUPPLEMENTARY NOTES N/A		12. SPONSORING MILITARY ACTIVITY Arnold Engineering Development Center Air Force Systems Command Arnold AF Station, Tennessee	
13. ABSTRACT This report presents heat-transfer measurements made on a typical satellite configuration in testing environments which simulate conditions at approximately 60 miles altitude, depending on full-scale vehicle size and the particular simulation parameter chosen. The total heating loads to various individual segments of the complete model are tabulated, and a heat-transfer distribution is proposed on the basis of the experimental results. Also reported are measurements on the effect of the extent of a cooled shroud on the heat transfer to a disk normal to the flow.			

14. KEY WORDS	LINK A		LINK B		LINK C	
	ROLE	WT	ROLE	WT	ROLE	WT
heat transfer earth satellites shrouded disks hypersonic flow wind tunnel tests low density tests						

INSTRUCTIONS

1. ORIGINATING ACTIVITY: Enter the name and address of the contractor, subcontractor, grantee, Department of Defense activity or other organization (*corporate author*) issuing the report.

2a. REPORT SECURITY CLASSIFICATION: Enter the overall security classification of the report. Indicate whether "Restricted Data" is included. Marking is to be in accordance with appropriate security regulations.

2b. GROUP: Automatic downgrading is specified in DoD Directive 5200.10 and Armed Forces Industrial Manual. Enter the group number. Also, when applicable, show that optional markings have been used for Group 3 and Group 4 as authorized.

3. REPORT TITLE: Enter the complete report title in all capital letters. Titles in all cases should be unclassified. If a meaningful title cannot be selected without classification, show title classification in all capitals in parenthesis immediately following the title.

4. DESCRIPTIVE NOTES: If appropriate, enter the type of report, e.g., interim, progress, summary, annual, or final. Give the inclusive dates when a specific reporting period is covered.

5. AUTHOR(S): Enter the name(s) of author(s) as shown on or in the report. Enter last name, first name, middle initial. If military, show rank and branch of service. The name of the principal author is an absolute minimum requirement.

6. REPORT DATE: Enter the date of the report as day, month, year; or month, year. If more than one date appears on the report, use date of publication.

7a. TOTAL NUMBER OF PAGES: The total page count should follow normal pagination procedures, i.e., enter the number of pages containing information.

7b. NUMBER OF REFERENCES: Enter the total number of references cited in the report.

8a. CONTRACT OR GRANT NUMBER: If appropriate, enter the applicable number of the contract or grant under which the report was written.

8b, 8c, & 8d. PROJECT NUMBER: Enter the appropriate military department identification, such as project number, subproject number, system numbers, task number, etc.

9a. ORIGINATOR'S REPORT NUMBER(S): Enter the official report number by which the document will be identified and controlled by the originating activity. This number must be unique to this report.

9b. OTHER REPORT NUMBER(S): If the report has been assigned any other report numbers (*either by the originator or by the sponsor*), also enter this number(s).

10. AVAILABILITY/LIMITATION NOTICES: Enter any limitations on further dissemination of the report, other than those

imposed by security classification, using standard statements such as:

- (1) "Qualified requesters may obtain copies of this report from DDC."
- (2) "Foreign announcement and dissemination of this report by DDC is not authorized."
- (3) "U. S. Government agencies may obtain copies of this report directly from DDC. Other qualified DDC users shall request through _____."
- (4) "U. S. military agencies may obtain copies of this report directly from DDC. Other qualified users shall request through _____."
- (5) "All distribution of this report is controlled. Qualified DDC users shall request through _____."

If the report has been furnished to the Office of Technical Services, Department of Commerce, for sale to the public, indicate this fact and enter the price, if known.

11. SUPPLEMENTARY NOTES: Use for additional explanatory notes.

12. SPONSORING MILITARY ACTIVITY: Enter the name of the departmental project office or laboratory sponsoring (*paying for*) the research and development. Include address.

13. ABSTRACT: Enter an abstract giving a brief and factual summary of the document indicative of the report, even though it may also appear elsewhere in the body of the technical report. If additional space is required, a continuation sheet shall be attached.

It is highly desirable that the abstract of classified reports be unclassified. Each paragraph of the abstract shall end with an indication of the military security classification of the information in the paragraph, represented as (TS), (S), (C), or (U).

There is no limitation on the length of the abstract. However, the suggested length is from 150 to 225 words.

14. KEY WORDS: Key words are technically meaningful terms or short phrases that characterize a report and may be used as index entries for cataloging the report. Key words must be selected so that no security classification is required. Identifiers, such as equipment model designation, trade name, military project code name, geographic location, may be used as key words but will be followed by an indication of technical context. The assignment of links, rules, and weights is optional.